Title Page

Isoform-specific biased agonism of histamine H₃ receptor agonists

Darren M Riddy, Anna E Cook, Natalie A Diepenhorst, Sanja Bosnyak, Ryan Brady,
Clotilde Mannoury la Cour, Elisabeth Mocaer, Roger J Summers, William N
Charman, Patrick M Sexton, Arthur Christopoulos, and Christopher J Langmead

*Drug Discovery Biology, Monash Institute of Pharmaceutical Sciences, Monash
University, Parkville, Victoria, Australia (D.M.R., A.E.C., N.D., S.B., R.B., R.J.S,
W.N.C, P.M.S., A.C., C.J.L.)*

*Institut de Recherches Internationales Servier, 50 Rue Carnot, 92284 Suresnes,
France (C.M.IC., E.M.)*

Running Title Page

Ligand-directed and isoform biased agonism at histamine H_3 receptors

Corresponding author

Dr Christopher J Langmead

Drug Discovery Biology, Monash Institute of Pharmaceutical Sciences, Monash University, 381 Royal Parade, Parkville, VIC, 3052, Australia

Tel. +61 3 990 39096

Email. chris.langmead@monash.edu

Number of text pages: 34

Number of tables: 2 and 2 supplementary

Number of figures: 7 and 2 supplementary

Number of references: 58

Number of words in the *Abstract*: 248

Number of words in the *Introduction*: 705

Number of words in the *Discussion*: 1454

Abbreviations

Imetit, 2-(1*H*-imidazol-5-yl)ethyl imidothiocarbamate, iodoproxyfan, 3-(1H-imidazol-4-yl)propyl-(4-iodophenyl)-methyl ether, proxyfan, 4-[3-(benzyloxy)propyl]-1*H*-imidazole, NαMH, N-α-methylhistamine dihydrochloride, pERK, phosphorylated extracellular signal-regulated kinase, RαMH, (R)(−)-α-methylhistamine dihydrochloride

Abstract

The human histamine H_3 receptor (hH_3R) is subject to extensive gene splicing that gives rise to a large number of functional and non-functional isoforms. Despite the general acceptance that G protein-coupled receptors can adopt different ligand-induced conformations that give rise to biased signalling, this has not been studied for the H_3R; further, it has unknown whether splice variants of the same receptor engender the same or differential biased signalling. Herein we have profiled the pharmacology of histamine receptor agonists at the two most abundant hH_3R splice variants (hH_3R_{445} and hH_3R_{365}) across seven signalling endpoints. Both isoforms engender biased signalling, notably for proxyfan (e.g. strong bias towards phosphorylation of GSK3β via the full-length receptor) and its congener iodoproxyfan, which are strongly consistent with the former's designation as a 'protean' agonist. The 80 amino acid IL3 deleted isoform, hH_3R_{365} is more permissive in its signalling than hH_3R_{445}: imetit, proxyfan and iodoproxyfan were all markedly biased away from calcium signalling and principal component analysis of the full dataset revealed divergent profiles for all five agonists. However, most interesting was the identification of differential biased signalling between the two isoforms. Strikingly, hH_3R_{365} was completely unable to stimulate GSK3β phosphorylation, an endpoint robustly activated by the full-length receptor. To the best of our knowledge, this is the first quantitative example of differential biased signalling *via* isoforms of the same G protein-coupled receptor that are simultaneously expressed *in vivo* and gives rise to the possibility of selective pharmacological targeting of individual receptor splice variants.

Introduction

It is now generally accepted that G protein-coupled receptors (GPCRs) can be stabilised into different receptor conformations by ligands to engender signalling bias towards some pathways to the relative exclusion of others (Kenakin, 2011; Kenakin & Christopoulos, 2013). Bias has been identified as a universal paradigm across family A, B and C GPCRs, exemplified, for instance, at the β_2-adrenergic receptor (Liu et al., 2012), parathyroid hormone-1 receptor (Gesty-Palmer et al., 2009), and the glucagon-like peptide-1 receptor (Koole et al., 2013), respectively. Biased agonism is now being exploited to develop compounds that preferentially target therapeutically relevant signalling pathways, and away from undesired endpoints, thus limiting on-target-mediated side effects (Valant et al., 2014; Nijmeijer et al., 2013).

The histamine H_3 receptor (H_3R) is a GPCR that is widely expressed in human brain with high levels localised to areas associated with cognition, such as the striatum, cerebral cortex and hippocampus (Pillot et al., 2002). It has been implicated in various pathologies, including Alzheimer's disease, schizophrenia, dementia, Parkinson's disease, depression and mood disorders (Barbier et al., 2007; Esbenshade et al., 2008; Bhowmik et al., 2012; Bitner et al., 2011, 2012), in part due to its function as an auto- and hetero-receptor, controlling the release of various neurotransmitters, including histamine, acetylcholine, dopamine, noradrenaline, GABA and glutamate (Gbahou et al., 2012). The receptor has also been associated with non-CNS conditions, such as multiple sclerosis, obesity and cancer (Berlin et al., 2011).

Due to its localisation and function, a number of selective H_3R agonists and antagonists have been developed, including imetit, proxyfan, thioperamide, ciproxifan, ABT-239, GSK-189254, JNJ-5207852 and pitolisant, (Barbier et al., 2004; Medhurst et al., 2007; Giannoni et al., 2010; Ligneau et al., 2007; Schwartz, 2011; Tiligada et al., 2009). Two H_3R ligands, proxyfan and cipralisant, were initially identified as inverse agonists, but later studies suggested that their pharmacology is more complex (Gbahou et al., 2003; Krueger et al.

4

2005). Explanations for their apparent 'protean' agonism include biased agonism, differential sensitivity to the stoichiometry and type of available G proteins expressed in the cell background, and/or differences in the level of constitutive activity present in the assay system (Gbahou et al., 2003; Kruger et al., 2005).

Moreover, and unlike other histamine receptor subtypes, the H_3R is subject to extensive splicing, yielding a large number of functionally active isoforms (Leurs et al., 2005). Of these, the full-length isoform, hH_3R_{445}, and the hH_3R_{365} version, are the most highly expressed within the human brain. Both isoforms display distinct localisation profiles, with hH_3R_{445} showing higher expression in the caudate, corpus callosum and spinal cord and hH_3R_{365} being predominant in several areas including the hypothalamus and cerebellum (Bongers et al., 2007). Interestingly, the 80 amino acid truncation comprises the C-terminal region of IL3 of the full-length receptor, implying that it could mediate differential coupling to intracellular effectors (Huang & Tesmer, 2011); a fact consistent with prior, sometimes conflicting, reports of the overall functionality of hH_3R_{365} (Coge et al., 2001; Wellendorph et al., 2002; Esbenshade et al., 2006; Bongers et al., 2007; Arrang et al., 2007).

Surprisingly, given the extensive number of probes and signalling pathways reported for the H_3R, there has been no systematic analysis of its ability to engender biased agonism, nor the impact of alternative splicing on such bias. Thus, the aim of the current study was to perform a comparative analysis of signalling to various pathways between the key hH_3R_{445} and hH_3R_{365} isoforms, thus focusing not only on "ligand-directed" biased agonism, but also on the potential for "isoform" bias. Strikingly, we identified marked differences in the signalling profile of the two receptor isoforms and notably, clear divergence in the ligand bias profile between the isoforms. Although previous studies have shown that naturally occurring mutations of the calcium-sensing receptor can give rise to differential signalling compared to the wild-type receptor (Leach et al., 2015), and a very recent paper described splice variant selectivity for the CXCR3 (Berchiche and Sakmar, 2016), to our knowledge, this is the first

quantitative assessment of differential agonist bias at isoforms of the same receptor that are

simultaneously expressed *in vivo*. This discovery could underlie some of the complex

pharmacology observed for H_3R ligands as well as impacting other therapeutic GPCRs targets

where multiple receptor isoforms are known to exist.

Materials and Methods

Cell line generation and culture

Stably expressed, tetracycline-inducible, Flp-In-CHO-TREx H_3R cell lines were generated as previously described by Ward et al., (2011). Clones were functionally screened for high expression as determined by the efficacy of imetit in 0.5 and 1 µg per mL tetracycline-treated cells in the inhibition of cAMP accumulation assay. Cell lines were maintained in DMEM: Ham's F-12 1:1 supplemented with 16mM HEPES, 5 µg per mL blasticidin, 300 µg per mL hygromycin B and 10% tetracycline free FBS at 37ºC/5% CO_2.

Membrane preparation

Cells were grown to 80-90 % confluence in 500 cm^2 cell-culture trays at 37ºC/5% CO_2. All subsequent steps were conducted at 4°C to avoid receptor degradation. The cell-culture medium was removed and ice-cold buffer (10 mL per tray; 10 mM HEPES, 0.9 % w/v NaCl, 0.2 % w/v EDTA, pH 7.4) was added to the cells. The cells were scraped from the trays into a 50 mL Corning tube and centrifuged at 250 x g for 5 min. The supernatant fraction was aspirated and 10 mL per 500 cm^2 tray of wash buffer (10 mM HEPES, 10 mM EDTA, pH 7.4) added to the pellet that was homogenized using an electrical homogenizer 'Werker, ultra-turrax' (position 6, 4 x 5 s bursts) and centrifuged at 48,000 x g at 4°C (Beckman Avanti J-251 Ultracentrifuge) for 30 min. The supernatant was discarded and the pellet re-homogenized in wash buffer and centrifuged as described above. The final pellet was suspended in ice-cold assay buffer (10 mM HEPES, 0.1 mM EDTA, pH 7.4) at a concentration of 1-2 mg per mL. Protein concentration was determined by a bicinchoninic acid assay, using BSA as a standard and aliquots maintained at -80°C until required.

[^{3}H]-*N*-α-methyl histamine binding

All radioligand experiments were conducted in 10 mL tubes, in assay binding buffer (50 mM Tris-HCL, 5 mM EDTA, pH 7.7) and at 25ºC. In all cases non-specific binding (NSB) was

determined in the presence of 10 μM ABT-239. After 1 h incubation, bound and free [^{3}H]-
*N*αMH were separated by rapid vacuum filtration using a FilterMate^{TM} Cell Harvester (Perkin
Elmer, Melbourne, Australia) onto 96-well GF/B filter mats presoaked with 0.3% PEI and
rapidly washed three times with ice cold wash buffer (50 mM Tris-HCL, 5 mM EDTA, pH
7.7). After drying (>1 h), filter mats were separated and placed into scintillation vials. To
these 2 mL of Ultima Gold (Perkin Elmer, Melbourne, Australia) was added and radioactivity
quantified using a liquid scintillation spectrometry, LS 6500 scintillation counter (Beckman
Coulter, High Wycombe, UK). Aliquots of [^{3}H]-*N*αMH were also quantified accurately to
determine how much radioactivity was added to each well. In all experiments, total binding
never exceeded more than 10 % of that added, limiting complications associated with
depletion of the free radioligand concentration.

**AlphaScreen™ SureFire™ Assays – Inhibition of cAMP accumulation, ERK1/2
phosphorylation (pERK1/2) and glycogen synthase kinase (GSK3β) pSer9**

The inhibition of cAMP accumulation and activation of pERK1/2 and GSK3β was measured
using AlphaScreen™ SureFire™ Assay Kits. Cells were seeded into transparent 96-well
plates at 40, 000 cells per well in the presence of 1 μg per mL tetracycline and incubated
overnight at 37ºC/5% CO$_2$. For the cAMP assay, cells were washed twice with PBS and
incubated in stimulation buffer (phenol red-free DMEM (GIBCO), 1% BSA and 1 mM 3-
isobutyl-1-methylxanthine), 37ºC/5% CO$_2$ for 1 h. For determination of agonist stimulated
concentration-response curves, cells were stimulated with compounds of interest for 10 min at
37ºC/5% CO$_2$ prior to addition of 3.16 μM forskolin and incubation at 37ºC/5% CO$_2$ for a
further 20 min. Media were removed and reactions terminated by addition of 50 μL per well
ice cold 100% ethanol. Cells were incubated at 22°C with shaking for 5 min prior to removal
of ethanol by evaporation. To the plate 100 μL per well of lysis buffer (0.1% BSA, 5 mM
HEPES, 0.3% Tween) was added followed by shaking for 5 min at 22°C. FBS was used as a
positive control for the pERK1/2 and GSK3β assays. Compounds were profiled in the

pERK1/2 assay using the time to peak as the agonist exposure time (generally 3 – 4 min).
These responses were terminated by the removal of drugs and addition of either 100 μL
(pERK1/2) or 25 μL (GSK3β) *SureFire*™ lysis buffer, and plates were agitated on a plate
shaker for 5 min. To determine agonist activity a volume of 5 μL (cAMP & pERK1/2) or 4
μL (GSK3β) cell lysate was added to a white Proxiplate™, followed by 10 μL (cAMP), 8 μL
(pERK1/2) or 5 μL (GSK3β) of 100:600:3:3 v/v/v/v mixture of *SureFire* activation
buffer/*SureFire* reaction buffer/AlphaScreen donor/acceptor beads. All plates were secured
with a top-seal. cAMP plates were incubated at 22 $^{\circ}$C overnight; pERK1/2 plates were
incubated at 37ºC/5% CO_2 for 1 h, and the GSK3β plates were incubated at 22ºC for 2 h. All
plates were incubated in the dark and fluorescence measured using a Fusion-Alpha or
Envision microplate reader (PerkinElmer, MA) using standard AlphaScreen settings.

[Ca^{2+}]$_i$-mobilization assays

Assays were performed in isotonic buffer (150 mM NaCl, 2.6 mM KCl, 2.2 mM $CaCl_2$, 1.18
mM $MgCl_2$, 10 mM D-glucose, 10 mM HEPES, 4 mM probenecid and 0.5 % w/v BSA, pH
7.4). Assay buffer was prepared as a [10x] stock (without probenecid or BSA), sterile filtered
and stored at 4 °C until required. A [1x] stock (500 mL) of assay buffer was prepared by
adding 50 mL of 10x stock and 5 mL of 400 mM probenecid (dissolved in 1 M NaOH) to 440
mL $H_2$0, and pH adjusted to 7.4, before making up the final volume to 500 mL. BSA (0.5 %
w/v) was added and [1x] assay buffer stored at 4°C for up to two weeks.

Cells were seeded into 96-well plates in growth medium at a density of 40, 000 cells per well
and treated with 1 μg per mL final tetracycline. The following day, plates containing a
confluent monolayer of cells were washed twice with 100 μL assay buffer, before being
loaded with 100 μL assay buffer containing 0.9 μM Fluo-4-AM. After 1 h incubation at
37ºC/5% CO_2, Fluo-4-AM containing buffer was removed and wells washed twice with 100
μL assay buffer, before being loaded with 180 μL assay buffer. After 20 min, compounds
were added on a Flexstation microplate reader (Molecular Devices; Sunnyvale, California).

9

Peak fluorescence was detected using 485 nm excitation and 525 nm emission filters. Data was normalised to the response to 100 µM ATP.

GTPγ^{35}S binding

Compounds were prepared at 100x final concentration in 100% DMSO, and 2.5 µL added to a 96-well assay plate. To each well, 200 µL of assay buffer, with 0.1% BSA and 30 µg per mL saponin added fresh on the day of experimentation, containing 50 µg per mL membranes, and 3.7 µM guanosine 5'-diphosphate sodium salt (GDP) was incubated at room temperature with gentle agitation for 30 min, allowing equilibrium to be reached. Following this, 50 µL of [^{35}S]-guanosine 5'-(γ-thio)triphosphate (GTPγ^{35}S) at a final concentration of 300 pM was added to each well and incubated at 22°C with gentle agitation for 40 min. Bound and free GTPγ^{35}S were separated by rapid vacuum filtration using a FilterMate^{TM} Cell Harvester (Perkin Elmer, Melbourne, Australia) onto 96-well GF/C filter plates and rapidly washed three times with ice cold wash buffer (50 mM Tris-HCL, 10 mM MgCl$_2$, 100 mM NaCl, pH 7.6). After drying (>4 h), 40 µL of Microscint^{TM} 20 (Perkin Elmer, Melbourne, Australia) was added to each well and radioactivity quantified using single photon counting on a MicroBeta^{2} microplate scintillation counter (Perkin Elmer, Melbourne, Australia).

[^{3}H]-arachidonic acid release – direct measurement of phospholipase (PLA2) activation

Cells were seeded into 96-well plates at a density of 40, 000 cells per well and receptor expression induced using 1 µg per mL tetracycline overnight at 37ºC/5% CO$_2$. The following day cells were washed with PBS and incubated with 0.25 µCi per mL of [^{3}H]-arachidonic acid in 1:1 DMEM:Ham's F12 containing 0.2% BSA for 2 h at 37ºC/5% CO$_2$. A time course was initially performed to determine the time at which [^{3}H]-arachidonic acid release peaked using 2 µM A23187, a Ca^{2+} ionophore, and 10 or 100 µM of agonist. Following incubation cells were washed and incubated for 10 min with agonists in 1:1 DMEM:Ham's F12 media.

After 10 min, 2 μM A23187 was added and cells incubated for further 20 min. [^{3}H]-arachidonic acid release was determined by liquid scintillation counting where, following incubation time, supernatant from each well was transferred to a new 96-well white Isoplate and IRGA-SAFE PLUS scintillant added. Plates were left for 30 min at room temperature and read on a MicroBeta^2 microplate scintillation counter (Perkin Elmer, Melbourne, Australia).

Label free technology (Cell impedance)

Experiments were conducted on a RTCA SP xCELLigence instrument (ACEA Biosciences) maintained at 37ºC/5% CO_2. Briefly, a blank read of 100 μL per well of medium was taken. Cells were seeded onto a 96-well E-plate at 20, 000 cells per well in the presence of 1 μg per mL tetracycline and allowed to settle for 30 min before replacing in the machine and monitoring every 2 min and then hourly overnight. Cells were washed with 100 μL per well PBS and 180 μL per well serum free medium added. Cells were then monitored every 15 sec for 1 h upon the addition of agonists at varying concentrations. Calculating the area under the cell impedance curves using the RTCA software 1.2, generated agonist concentration-response curves using medium only wells as baseline.

Compounds and reagents

All compounds were supplied from Sigma Aldrich, Castle Hill, Australia (R-α-methylhistamine, N-α-methylhistamine); Servier, Paris, France (imetit, proxyfan), or synthesized in-house (iodoproxyfan; as described in Stark et al., 1996). Radioligands were supplied by Perkin Elmer, Melbourne, Australia. Cell culture and molecular biology reagents were supplied by Life Technologies, Melbourne, Australia.

Data analysis

Saturation binding isotherms were analysed by non-linear regression according to a hyperbolic, one-site binding model, and individual estimates for total receptor number (B$_{max}$)

and radioligand dissociation constant (K_D) were calculated. The following equation was used, where [A] is the concentration of radioligand:

$$Y = \frac{B_{max}\,[A]}{K_D + [A]} \qquad (1)$$

Agonist concentration-response curves were fitted to sigmoidal three-parameter logistic equation:

$$Y = Basal + \frac{(E_{max} - Basal)}{1 + 10^{\wedge}(LogEC_{50} - X)} \qquad (2)$$

where Y is the response measured. E_{max} denotes maximal asymptotic response and Basal denotes minimal asymptotic response.

The analysis of the same datasets to quantify biased agonism can be undertaken in a number of ways; transducer ratios ($Log(\tau/K_A)$), relative activity (RA) ratios ($\Delta Log(E_{max}/EC_{50})$) and relative potency ratios (ΔpEC_{50}; Kenakin et al., 2012). As not all ligands were full agonists in each system (necessary for simple calculation of relative potency ratios), relative transducer ratios were used as the measure of bias. Data from each individual experiment for each pathway were fitted to an equation that directly estimates $Log(\tau/K_A)$ and avoids propagation of error associated with fitting individual E_{max} and EC_{50} values using the standard Hill equation:

$$Response = basal + \frac{(E_m - Basal)\left(\frac{\tau}{K_A}\right)^n [A]^n}{[A]^n \left(\frac{\tau}{K_A}\right)^n + \left(1 + \frac{[A]}{K_A}\right)^n} \qquad (3)$$

where E_m is the maximal response of the system, *Basal* is the level of the response in the absence of agonist, K_A denotes the equilibrium dissociation constant of the agonist *A*; τ/K_A (determined as a logarithm; Christopoulos, 1998) is a composite parameter sufficient to describe agonism and bias for a given pathway, i.e., stimulus-biased agonism can result from either a selective affinity (K_A) of an agonist for a given receptor state(s) and/or a differential coupling efficacy (τ) toward certain pathways, where τ is an index of the signalling efficacy of the agonist (defined as R_T/K_E, where R_T is the total number of receptors and K_E is the coupling efficiency of each agonist-occupied receptor), and n is the slope of the transducer function.

To remove system bias, $\text{Log}(\tau/K_A)$ values were normalised to the reference agonist RαMH. The $\Delta\text{Log}(\tau/K_A)$ value was determined for each ligand for each pathway was normalized to the RαMH response in the same pathway, according to the following equation:

$$\Delta\text{Log}\left(\frac{\tau}{K_A}\right) = \text{Log}\left(\frac{\tau}{K_A}\right)_{test\ ligand} - \text{Log}\left(\frac{\tau}{K_A}\right)_{R\alpha MH} \tag{4}$$

To account for the differences in expression (R_T) of hH$_3$R$_{365}$ and hH$_3$R$_{445}$, τ/K_A values for agonists at hH$_3$R$_{365}$ were normalised using the ratio of maximal binding capacity (B_{max}) values from saturation binding isotherms of [^{3}H]-*N*-α-methyl-histamine ([^{3}H]-NαMH; correction factor = 3.36; *vide infra*, and shown in Supplementary Figure 1).

The standard error of the mean (SEM) for each $\Delta\text{Log}(\tau/K_A)$ value within the same pathway was calculated according to the following equation:

$$Pooled\ SEM = \sqrt{\left(\text{SEM}_{test\ ligand}\right)^2 + \left(\text{SEM}_{R\alpha MH}\right)^2} \tag{5}$$

13

To account for observational bias the calculated $\Delta\text{Log}(\tau/K_A)$ values were further normalised

to the reference pathway, cAMP. The $\Delta\Delta\text{Log}(\tau/K_A)$ value was determined as above using the

following equation:

$$\Delta\Delta\text{Log}\left(\frac{\tau}{K_A}\right) = \Delta\text{Log}\left(\frac{\tau}{K_A}\right)_{test\ pathway} - \Delta\text{Log}\left(\frac{\tau}{K_A}\right)_{cAMP} \tag{6}$$

The standard error of the mean (SEM) for each $\Delta\Delta\text{Log}(\tau/K_A)$ value were calculated as before:

$$Pooled\ SEM = \sqrt{\left(\text{SEM}_{test\ pathway}\right)^2 + \left(\text{SEM}_{cAMP}\right)^2} \tag{7}$$

Differences amongst $\Delta\text{Log}(\tau/K_A)$ values were compared according to a two-way ANOVA

(with assay and agonist as the two group variables) with multiple planned comparisons using

Tukey's test (i) between pathways for the same agonist and (ii) between agonists for the same

pathway.

To investigate whether any agonist, at anyway pathway, was biased towards either of the two

receptor isoforms, $\Delta\text{Log}(\tau/K_A)_{445\text{-}365}$ values were calculated using the following equation:

$$\Delta\text{Log}\left(\frac{\tau}{K_A}\right)_{445-365} = \text{Log}\left(\frac{\tau}{K_A}\right)h\,H_3R_{445} - \text{Log}\left(\frac{\tau}{K_A}\right)h\,H_3R_{365} \tag{8}$$

$\Delta\text{Log}(\tau/K_A)_{445\text{-}365}$ values were compared to a theoretical value of zero (i.e. no isoform bias)

using a one-sample T-test.

Principal component analysis (PCA) was subsequently applied to the calculated $\Delta\Delta\text{Log}(\tau/K_A)$

bias values obtained in eq. 8 for both isoforms, using singular value decomposition as

implemented in the package scikit-learn (Pedregosa et al., 2011). This analysis is a

dimensionality reduction method that uses transformations to project a high-dimensional set

14

of data into a lower dimensional set of variables, called principal components (PCs) (Thompson et al., 2015). The extracted PC values contain important information from the data, revealing its internal structure in a way that best explains its variance (Wold et al., 1987). PCs are ranked according to the percentage of total variance in the data they explain. PC1 explains the maximal total variance found within the data. The subsequent PC values represent the remaining variation, without being correlated with the preceding components. The script used for the analysis and plotting can be found at https://github.com/thomas-coudrat/pca_analysis.

Results

Expression and assay development for histamine H$_3$ receptor isoforms

To compare the pharmacology of the two most abundantly expressed human histamine H$_3$ receptor isoforms, CHO-TREx cell lines stably expressing either hH$_3$R$_{365}$ or hH$_3$R$_{445}$ were generated. [^{3}H]-NαMH saturation binding isotherms were monophasic for both isoforms and revealed that the hH$_3$R$_{445}$ isoform (B_{max} = 2541 ± 77 fmol/mg protein) was expressed at over three times the level of the hH$_3$R$_{365}$ isoform (B_{max} = 757 ± 52 fmol/mg protein; exact ratio 3.36; Supplementary Figure 1), with no significant difference in affinity (pK$_D$ values 8.90 ± 0.30 and 8.80 ± 0.90, respectively; grouped data are shown ± SEM (n=3)).

Concentration-response curves to each of the five histamine receptor agonists (RαMH, imetit, NαMH, proxyfan and iodoproxyfan; Figure 1) were generated in functional assays of (i) inhibition of forskolin-stimulated cAMP accumulation, (ii) [Ca^{2+}]$_i$-mobilization, (iii) ERK1/2 phosphorylation, (iv) GTPγ^{35}S binding, (v) PLA$_2$ activity ([^{3}H]-arachidonic acid release), (vi) GSK3β phosphorylation and (vii) cell impedance. Somewhat surprisingly, all agonist-evoked responses at both isoforms were blocked by an overnight treatment with pertussis toxin (PTX; 10 ng / mL), indicating that all downstream signalling was via G$_{i/o}$ protein-coupling (*data not shown*).

Generally, all five compounds displayed agonist activity in all signalling assays and at both isoforms, with potencies being approximately 10-fold higher at the hH_3R_{445} isoform compared to hH_3R_{365} (Figures 2 & 3; Supplementary Tables 1 & 2), in part reflecting the higher expression of the former. For hH_3R_{445}, agonists were most potent for the inhibition of cAMP accumulation and GSK3β phosphorylation (Figure 2; Table 1), with a general rank order of potencies being inhibition of cAMP accumulation = GSK3β > pERK1/2 = PLA_2 = $GTP\gamma^{35}S$ binding > $[Ca^{2+}]_i$-mobilization > cell impedance (Figure 2; Supplementary Table 1). At hH_3R_{365} a similar profile was observed across most assays, although strikingly this isoform was completely unable stimulate the phosphorylation of GSK3β, the most sensitive assay for hH_3R_{445} (Figure 3; Supplementary Table 2). More subtly, the potencies to promote $GTP\gamma^{35}S$ binding were closer to those obtained in the inhibition of cAMP accumulation assay compared to hH_3R_{445}; the general rank order of potency being: inhibition of cAMP accumulation > $GTP\gamma^{35}S$ binding > PLA2 = pERK1/2 > $[Ca^{2+}]_i$-mobilization > cell impedance (Figure 3; Supplementary Table 2).

In general, RαMH and NαMH behaved as full agonists in all assays and at both isoforms (with the exception of NαMH in the inhibition of cAMP accumulation assay; Figures 2 & 3). However, imetit, proxyfan and iodoproxyfan yielded more variable responses, with different rank orders of activity across assays and partial agonist versus full agonist behaviours (Figures 2 & 3). Agonist responses at both receptor isoforms were quantitatively assessed using the transducer ratio method (Kenakin et al., 2012) to determine biased agonism both within and between isoforms.

Evaluation of biased agonism at the full-length histamine H₃ receptor

For both isoforms RαMH was used as the reference agonist to calculate $\Delta Log(\tau/K_A)$ values (Tables 1 & 2; Figures 4 & 5A, B); these values were normalised to the inhibition of cAMP accumulation as the reference pathway to generate $\Delta\Delta Log(\tau/K_A)$ values (Tables 1 & 2; Figure 5C,D). Interestingly, NαMH, a regioisomer of RαMH, displayed no significant biased

16

signalling at hH_3R_{445} (Table 1; Figures 4 & 5). Imetit followed a similar pattern, although when the dataset is normalised to the inhibition of cAMP (i.e. $\Delta\Delta Log(\tau/K_A)$), it displayed clear bias towards GSK3β (36-fold) and ERK1/2 (12-fold) phosphorylation (Table 1; Figure 5c).

Perhaps unsurprisingly, proxyfan, the 'protean' agonist of the histamine H_3 receptor, displayed a much more varied profile; it was significantly biased away from the inhibition of cAMP, trending in the same direction for calcium mobilization, ERK1/2 phosphorylation and $GTP\gamma^{35}S$ binding. Given the relative lack of activity to inhibit cAMP accumulation, when the data were normalised to this pathway, proxyfan displayed marked bias towards GSK3β phosphorylation (260-fold), changes in cellular impedance (28-fold) and ERK1/2 phosphorylation (6.6-fold; Table 1; Figure 5C). Iodoproxyfan also displayed significant bias towards a change in cell impedance, a response that was itself significantly different to its ability to inhibit forskolin-stimulated cAMP accumulation at the hH_3R_{445} isoform. When normalised to the latter, marked bias towards changes in cellular impedance (150-fold) and GSK3β phosphorylation (33-fold) were evident (Table 1; Figure 5C).

Evaluation of biased agonism at the IL3 deleted histamine H_3 receptor

Our subsequent study sought to determine whether the 80 amino acid deleted receptor, hH_3R_{365} could also mediate biased agonism. Overall, this isoform appeared more permissive in its signalling than the full-length receptor (Figures 4 & 5; Table 2). Two-way ANOVA of resultant $\Delta Log(\tau/K_A)$ values in Table 2 revealed a highly significant effect of agonists ($P < 0.0001$) and assay ($P < 0.0001$), but also a very significant interaction between the two variables ($P = 0.0008$), an effect absent at hH_3R_{445} ($P = 0.22$; Figure 4).

Although NαMH displayed no substantial differences compared to the reference agonist RαMH, the profiles of imetit, proxyfan and iodoproxyfan were highly divergent, confirming the presence of significant bias downstream of the receptor (Table 2; Figures 4B & 5B, D).

Imetit was significantly (74-fold) biased towards the inhibition of cAMP accumulation relative to RαMH. Normalisation of the responses to this pathway revealed that imetit was markedly biased *away* from calcium mobilization (0.007-fold), cellular impedance (0.01-fold), GTPγ^{35}S binding (0.07-fold) and ERK1/2 phosphorylation (0.1-fold).

Interestingly, proxyfan and iodoproxyfan were unable to evoke, and hence highly biased away from, calcium mobilization responses at the hH$_3$R$_{365}$ isoform, despite robust responses to RαMH, NαMH and imetit (Table 2; Figure 4B; Supplementary Table 2). Accordingly, their activity relative to RαMH was fixed to an arbitrary ΔLog(τ/K_A) value of -3.0. This extreme bias away from calcium mobilization for proxyfan and its congener was notable as it was the only functional endpoint for which either compound displayed bias relative to RαMH (all other pathways, bar pERK1/2 for proxyfan, were significantly different to the fixed ΔLog(τ/K_A) values of -3.0 for both agonists; Figure 4B). Even when normalised to cAMP as a reference pathway, only iodoproxyfan exhibited any other biased agonism, being biased away from ERK1/2 phosphorylation (0.04-fold; Table 2; Figures 4B & 5B, D).

The histamine H$_3$ receptor exhibits 'isoform bias'

Although both the full length and 80 amino acid deleted H$_3$R mediate biased agonism, it remained to be determined whether the direction and magnitude of the bias was conserved *between* isoforms. Strikingly, none of the agonists stimulated GSK3β phosphorylation *via* hH$_3$R$_{365}$, a pathway readily activated by the hH$_3$R$_{445}$ isoform, indicating that the hH$_3$R$_{365}$ isoform is highly biased away from this endpoint (though no quantification was possible due to the lack of activity of any ligand).

Even for pathways activated by both isoforms, visual inspection of the "webs of bias" in Figure 5 suggests that the pharmacology of the hH$_3$R$_{445}$ and hH$_3$R$_{365}$ isoforms is different. In order to test this assertion, Log(τ/K_A) values for each agonist in each assay at hH$_3$R$_{365}$ were subtracted from the corresponding values at the hH$_3$R$_{445}$ isoform (Figure 6). A value that is

18

not significantly different from zero suggests that the agonist is equi-effective at both receptor isoforms.

Individual one-sample T-tests for the values reveal a number of significant examples of isoform bias. Proxyfan and iodoproxyfan only promoted calcium mobilization *via* the hH_3R_{445} isoform; whereas RαMH was approximately 13-fold more effective at inhibiting cAMP levels at this isoform compared to hH_3R_{365}. However, imetit was significantly more efficient at promoting G protein coupling (GTPγ^{35}S binding) at the hH_3R_{365} isoform (Figure 6). Given the subtle differences in localisation and function of the two major isoforms of the H_3 receptor, choice of agonist could influence the observed response(s) and may represent a novel route to selective pharmacology.

To ensure that receptor desensitization or internalization did not markedly influence the bias analysis across the two isoforms, concentration response curves to each agonist were constructed at varying incubation times using the cAMP assay (data not shown). At the 10 min time point that we routinely used for agonist incubations, only minimal desensitisation was observed for both receptor isoforms, and appeared comparable for all agonists tested (% response to 10 μM agonist compared to the 2 min time point, ranging from 76.4 ± 1.8 to 87.6 ± 5.6 and 82.2 ± 6.1 to 92.2 ± 2.3 for the hH_3R_{445} and hH_3R_{365} isoforms respectively; Supplementary Figure 2a & b). In addition, ΔLogτ/K_A values (with reference to RαMH) were calculated and did not significantly change over time (Supplementary Figure 2c & d).

Principal component analysis

The bias factors ($\Delta\Delta$Log(τ/K_A)) for the two receptor isoforms were then subjected to PCA, a dimensionality reduction method, to reveal values in the dataset that contribute variability between ligands. Ligands that display similar behaviour cluster together. At hH_3R_{445}, NαMH clustered most closely with RαMH (in PC1), clearly separated from proxyfan, and to a lesser

degree iodoproxyfan (Figure 7A). The composite of both PC1 (83%) and PC2 (10%) accounted for 93% of the total variability, indicating limited variation within this dataset. This simple representation reflects what is intuitively visualised in the "web of bias" for hH_3R_{445} (Figure 5C).

Consistent with the more variable pharmacology and permissive signalling of hH_3R_{365}, there was no evidence of ligand clustering, suggesting that all ligands produce different bias profiles at this isoform, again correlating with their corresponding bias plots (Figure 5D; Figure 7B). Indeed, comparison of the two principal component analysis plots intuitively reveals the "isoform bias" that exists between hH_3R_{445} and hH_3R_{365}.

Discussion

Although the histamine H_3 receptor has long been a therapeutic target of considerable interest, its ability to engender biased signalling has not been comprehensively investigated. Herein we have demonstrated that not only can agonists give rise to biased signalling ("ligand-directed bias"), but that two most abundant human H_3R splice variants (hH_3R_{445} and hH_3R_{365}) engender different responses ("isoform bias").

The regioisomeric agonists, RαMH and NαMH, display similar pharmacology with no bias at the hH_3R_{445} isoform. The structurally related agonist, imetit, also had a similar profile, though analysis revealed bias towards phosphorylation of GSK3β and ERK1/2. Strikingly, proxyfan, as well its congener iodoproxyfan, produce clearly divergent signalling at the full-length H_3R with marked bias towards GSK3β phosphorylation and changes in cellular impedance (Figures 4 & 5). Their distinct profile, both compared to the histamine analogues as well as each other, is reflected in a PCA of the bias factors (Figure 7A).

The quantitative confirmation of biased agonism with proxyfan (and iodoproxyfan) helps to explain previous studies that have variously described proxyfan as an inverse agonist, antagonist, partial agonist or full agonist due to its context-dependent pharmacology (Gbahou et al., 2003; Krueger et al., 2005). This compound's protean agonism has been previously attributed to the degree of constitutive receptor activity present in the assay system under test (Bongers et al., 2007; Morisset et al., 2000). However, in our studies constitutive activity was only evident at hH_3R_{445} in the inhibition of cAMP accumulation and $GTP\gamma^{35}S$ binding assays (*data not shown*), suggesting that constitutive activity does not appear to influence the bias that proxyfan engenders.

The second aim of this study was to determine the bias profile of the most abundant isoform of the histamine H_3 receptor, hH_3R_{365}. This splice variant was also subject to biased agonism; notably neither proxyfan nor iodoproxyfan stimulated calcium mobilization *via* hH_3R_{365}, despite robust responses to NαMH and RαMH (Figure 3; Table 2). Overall, the profiles of imetit, proxyfan and iodoproxyfan across the endpoints tested were distinct both to NαMH, RαMH and each other, confirming that this isoform is permissive in its signalling, an assertion supported by the lack of clustering of ligands in the PCA (Figure 7B) and the highly significant interaction between ligands and assays in the two-way ANOVA of the $\Delta Log(\tau/K_A)$ values for hH_3R_{365} (Figure 4).

The molecular basis of biased agonism for the hH_3R is unclear. Many prominent examples of biased agonism distinguish between G protein-dependent and -independent signalling (Kenakin & Christopoulos, 2013), but herein we have found that all of the functional responses are sensitive to prior treatment of the cells with PTX, implying that all of the signalling is downstream of the $G_{i/o}$ family of G proteins. As such, the observed biased agonism may arise from activation of different Gα or Gβγ subunits, as previously

demonstrated for the β_3-adrenoceptor (Sato et al., 2007), or variations in drug-receptor kinetics.

The latter is emerging as a key consideration in GPCR discovery, rationalising *in vivo* efficacy, drug duration of action and selectivity (Riddy et al., 2015; Hoffmann et al., 2015; Copeland, 2016). More recent studies have also implicated the kinetics of signalling as a key component of biased agonism (Klein Herenbrink et al., 2016). Given that the assays described herein measure endpoints that range from 15 seconds (calcium mobilization) to 60 minutes (cellular impedance), temporal differences could underlie the observed signalling profiles for proxyfan and iodoproxyfan. Previous studies have shown that intrinsic efficacy of muscarinic M_3 receptor (mAChR) agonists correlate with their dissociation rates; agonists that displayed slow dissociation had higher efficacy in calcium mobilization and GTPγ^{35}S binding assays (Sykes et al., 2009). Therefore, the bias profiles of proxyfan and iodoproxyfan could be due to differential receptor binding kinetics when compared to the simpler histamine analogues, though determination of such properties is beyond the scope of this study. Interestingly, the different lengths of incubation of the signalling assays presented here could explain why the observed bias at the hH_3R_{445} isoform in this study contrasts with that of Schnell et al., (2010), in which the same agonists displayed no bias when assessed by steady-state GTPase activity with various co-expressed G proteins in Sf9 insect cells.

Further to the identification of biased agonism at H_3R splice variants, we then sought to compare the bias profiles of the two isoforms (appropriately corrected for differences in receptor expression). Unexpectedly, there was a striking difference in signalling between the two major splice variants, which we have termed "isoform bias". Despite the absence of 80 amino acids in the third intracellular loop in hH_3R_{365} (Bongers et al., 2007; Leurs et al., 2005) and the importance of this region in G protein coupling (O'Dowd et al., 1988), hH_3R_{365} elicits G protein-dependent signalling. Nonetheless, this truncation results in a receptor that robustly couples to some pathways (e.g. inhibition of cAMP accumulation, GTPγ^{35}S binding), as for

hH$_3$R$_{445}$, but which is completely unable to activate others (GSK3β phosphorylation) and only

permissively links to further pathways (e.g. RαMH vs. proxyfan in calcium mobilization).

This striking "isoform bias" between the two variants was quantified by calculation of the

difference in Log(τ/K_A) values for each agonist at each pathway, and revealed a general

preference for imetit to activate pathways downstream of the hH$_3$R$_{365}$ isoform, with

iodoproxyfan and proxyfan favouring the full length receptor (Figure 6).

The cause of the differential pharmacology between hH$_3$R$_{445}$ and hH$_3$R$_{365}$ isoforms is not

clear; previous studies using G protein-coupled inward rectifier potassium channel (GIRK)

activation as a surrogate of receptor activation showed that the hH$_3$R$_{365}$ isoform yielded GIRK

responses with a 5-6-fold increase in deactivation kinetics compared to hH$_3$R$_{445}$, implying that

agonists may have a slower off-rate from this isoform (Sahlholm et al., 2012). It could also be

that the kinetic rate(s) of GDP/GTP exchange may differ between isoforms (Dror et al.,

2015). An alternative explanation could be that the differences arise due to a change in the

distances between transmembrane (TM) domains 5 and 6 between isoforms. Kruse et al.,

(2012) demonstrated, using all known inactive GPCR structures, that the distance between the

bases of TM5 and TM6 of Gα$_{i/o}$-coupled receptors ranged between 12.5 and 14.5Å, whilst, for

Gα$_s$-coupled receptors this distance was shorter, ranging from 10 to 12Å. The distance

between TM5 and TM6 for the hH$_3$R$_{365}$ isoform may be reduced, resulting in a receptor that

differentially couples to G protein isoforms, in turn activating different signalling networks.

Irrespective of mechanism, the "isoform bias" identified is potentially of therapeutic

relevance. Previous studies have extended analysis of biased signalling to naturally occurring

mutant variants of the G protein-coupled calcium-sensing receptor, demonstrating significant

changes in the signalling profile that, in part, account for their role in various endocrine

diseases (Leach et al., 2015). These data demonstrated that even single amino acid changes

result in different receptor conformation that give rise to biased signalling. Unsurprisingly

23

therefore, the more significant changes in amino acid sequence resulting from gene splicing for the H_3R readily yields change in biased signalling profile. Nevertheless, we believe that this is the first example of differential signalling mediated by splice variants of the same G protein-coupled receptor. Given that these histamine receptor isoforms have subtly different expression profiles in the brain, further experiments are required to determine whether the observed bias links to CNS diseases - for example in which both GSK3β and the histamine H_3 receptor have been implicated, such as schizophrenia and Alzheimer's disease (Hooper et al., 2008; DaRocha-Souto et al., 2012; Cole, 2013). Studies in rat tissue have suggested that the well-described auto-receptor function of the histamine H_3 receptor to control histamine release may be mediated primarily by a truncated isoform (Gbahou et al., 2012), implying that the hH_3R_{365} isoform could play this role in humans. If this were to be the case, the differential activation of downstream effector systems may have evolved to be an auto-receptor-specific mechanism; the data herein offer the possibility that it might be possible to design drugs that selectively target individual H_3R isoforms. This also may have implications for other receptors for which known variants exist and biased agonism or allosteric modulation has been previously documented e.g. dopamine D_2 receptors (Shonberg et al., 2013; Weichert et al., 2015) and mGlu5 receptors (Noetzel et al., 2013; Rook et al., 2015).

In summary, a cross-wise evaluation of five agonists at multiple signalling pathways downstream the two main histamine H_3 receptor isoforms clearly identified significant ligand-directed biased signalling, most notably for proxyfan, corroborating previous studies describing this compound as a protean agonist. However, even more striking was the identification of "isoform bias" in our study, to our knowledge the first quantitative evidence of this phenomenon in the GPCR field. Whilst the aetiology of the differential bias is not yet clear, it may help guide future discovery efforts targeting the histamine H_3 receptor.

Acknowledgements

Authorship Contributions

Participated in research design: Riddy, Cook, Mannoury la Cour, Mocaer, Summers, Sexton,

Christopoulos, Langmead

Conducted experiments: Riddy, Cook, Diepenhorst, Bosnyak

Contributed new reagents or analytic tools: Brady

Performed data analysis: Riddy, Cook, Diepenhorst, Bosnyak, Langmead

Wrote or contributed to the writing of the manuscript: Riddy, Summers, Charman, Sexton,

Christopoulos, Langmead

References

Arrang J-M, Morisset S, and Gbahou F (2007). Constitutive activity of the histamine H3 receptor. *Trends Pharmacol Sci* **28**(7):350–357.

Barbier AJ, Berridge C, Dugovic C, Laposky AD, Wilson SJ, Boggs J, Aluisio L, Lord B, Mazur C, Pudiak CM et al., (2004). Acute wake-promoting actions of JNJ-5207852, a novel, diamine-based H3 antagonist. *Br J Pharmacol* **143**:649–661.

Barbier AJ, Aluisio L, Lord B, Qu Y, Wilson SJ, Boggs JD, Bonaventure P, Miller K, Fraser I, Dvorak L et al., (2007). Pharmacological characterization of JNJ-28583867, a histamine H(3) receptor antagonist and serotonin reuptake inhibitor. *Eur J Pharmacol* **576**:43–54.

Berchiche YA, and Sakmar TP (2016). CXC Chemokine Receptor 3 Alternative Splice Variants Selectively Activate Different Signaling Pathways. *Mol Pharmacol* **90**:483–495.

Berlin M, Boyce CW, and Ruiz M de L (2011). Histamine H3 receptor as a drug discovery target. *J Med Chem* **54**:26–53.

Bhowmik M, Khanam R, and Vohora D (2012). Histamine H3 receptor antagonists in relation to epilepsy and neurodegeneration: a systemic consideration of recent progress and perspectives. *Br J Pharmacol* **167**:1398–1414.

Bitner RS, Markosyan S, Nikkel AL, and Brioni JD (2011). In-vivo histamine H3 receptor antagonism activates cellular signaling suggestive of symptomatic and disease modifying efficacy in Alzheimer's disease. *Neuropharmacology* **60**:460–466.

Bitner RS (2012). Cyclic AMP response element-binding protein (CREB) phosphorylation: a mechanistic marker in the development of memory enhancing Alzheimer's disease therapeutics. *Biochem Pharmacol* **83**:705–714.

Bongers G, Krueger KM, Miller TR, Baranowski JL, Estvander BR, Witte DG, Strakhova MI, van Meer P, Bakker RA, Cowart MD et al., (2007). An 80-amino acid deletion in the third intracellular loop of a naturally occurring human histamine H3 isoform confers

26

pharmacological differences and constitutive activity. *J Pharmacol Exp Ther* **323**:888–898.

Christopoulos A (1998). Assessing the distribution of parameters in models of ligand-receptor interaction: to log or not to log. *Trends Pharmacol Sci* **19**:351–357.

Cogé F, Guénin SP, Audinot V, Renouard-Try A, Beauverger P, Macia C, Ouvry C, Nagel N, Rique H, Boutin JA et al., (2001). Genomic organization and characterization of splice variants of the human histamine H3 receptor. *Biochem J* **355**:279–288.

Cole AR (2013). Glycogen synthase kinase 3 substrates in mood disorders and schizophrenia. *FEBS J* **280**:5213–5227.

Copeland R A (2016). The drug-target residence time model: a 10-year retrospective. *Nat Rev Drug Discov*.

DaRocha-Souto B, Coma M, Pérez-Nievas BG, Scotton TC, Siao M, Sánchez-Ferrer P, Hashimoto T, Fan Z, Hudry E, Barroeta I et al., (2012). Activation of glycogen synthase kinase-3 beta mediates β-amyloid induced neuritic damage in Alzheimer's disease. *Neurobiol Dis* **45**:425–437.

Dror RO, Mildorf TJ, Hilger D, Manglik A, Borhani DW, Arlow DH, Philippsen A, Villanueva N, Yang Z, Lerch MT (2015). Structural basis for nucleotide exchange in heterotrimeric G proteins. *Science* **348**:1361–1365.

Esbenshade TA, Krueger KM, Yao BB, Witte DG, Estvander BR, Baranowski JL, Miller TR, and Hancock AA (2006). Differences in pharmacological properties of histamine H(3) receptor agonists and antagonists revealed at two human H (3) receptor isoforms. *Inflamm res* **55** Suppl 1:S45–6.

Esbenshade TA, Browman KE, Bitner RS, Strakhova M, Cowart MD, and Brioni JD (2008). The histamine H3 receptor: an attractive target for the treatment of cognitive disorders. *Br J Pharmacol* **154**:1166–1181.

Gbahou F, Rouleau A, Morisset S, Parmentier R, Crochet S, Lin J-S, Ligneau X, Tardivel-Lacombe J, Stark H, Schunack W et al., (2003). Protean agonism at histamine H3 receptors in vitro and in vivo. *Proc. Natl. Acad. Sci. U.S.A.* **100**:11086–11091.

27

Gbahou F, Rouleau A, and Arrang J-M (2012). The histamine autoreceptor is a short isoform of the H₃ receptor. *Br J Pharmacol* **166**:1860–1871.

Gesty-Palmer D, Flannery P, Yuan L, Corsino L, Spurney R, Lefkowitz RJ, and Luttrell LM (2009). A beta-arrestin-biased agonist of the parathyroid hormone receptor (PTH1R) promotes bone formation independent of G protein activation. *Sci Transl Med* **1**(1): 1ra1.

Giannoni P, Medhurst AD, Passani MB, Giovannini MG, Ballini C, Corte LD, and Blandina P (2010). Regional differential effects of the novel histamine H3 receptor antagonist 6-[(3-cyclobutyl-2,3,4,5-tetrahydro-1H-3-benzazepin-7-yl)oxy]-N-methyl-3-pyridinecarboxamide hydrochloride (GSK189254) on histamine release in the central nervous system of freely moving rats. *J Pharmacol Exp Ther* **332**:164–172.

Hoffmann C, Castro M, Rinken A, Leurs R, Hill SJ, and Vischer HF (2015). Ligand Residence Time at G-protein-Coupled Receptors-Why We Should Take Our Time To Study It. *Mol Pharmacol* **88**:552–560.

Hooper C, Killick R, and Lovestone S (2008). The GSK3 hypothesis of Alzheimer's disease. *J Neurochem* **104**:1433–1439.

Huang C-C, and Tesmer JJG (2011). Recognition in the face of diversity: interactions of heterotrimeric G proteins and G protein-coupled receptor (GPCR) kinases with activated GPCRs. *J Biol Chem* **286**:7715–7721.

Kenakin T (2011). Functional selectivity and biased receptor signaling. *J Pharmacol Exp Ther* **336**:296–302.

Kenakin T, Watson C, Muniz-Medina V, Christopoulos A, and Novick S (2012). A simple method for quantifying functional selectivity and agonist bias. *ACS Chem Neurosci* **3**:193–203.

Kenakin T, and Christopoulos A (2013). Signalling bias in new drug discovery: detection, quantification and therapeutic impact. *Nat Rev Drug Discov* **12**:205–216.

Klein Herenbrink C, Sykes DA, Donthamsetti P, Canals M, Coudrat T, Shonberg J, Scammells PJ, Capuano B, Sexton PM, Charlton SJ, Javitch JA, Christopoulos A, and

Lane JR (2016). The role of kinetic context in apparent biased agonism at GPCRs. *Nat Commun* **7**:10842.

Koole C, Savage EE, Christopoulos A, Miller LJ, Sexton PM, and Wootten D (2013). Minireview: Signal bias, allosterism, and polymorphic variation at the GLP-1R: implications for drug discovery. *Mol Endocrinol* **27**:1234–1244.

Krueger KM, Witte DG, Ireland-Denny L, Miller TR, Baranowski JL, Buckner S, Milicic I, Esbenshade TA, and Hancock AA (2005). G protein-dependent pharmacology of histamine H3 receptor ligands: evidence for heterogeneous active state receptor conformations. *J Pharmacol Exp Ther* **314**:271–281.

Kruse AC, Hu J, Pan AC, Arlow DH, Rosenbaum DM, Rosemond E, Green HF, Liu T, Chae PS, Dror RO et al., (2012). Structure and dynamics of the M3 muscarinic acetylcholine receptor. *Nature* **482**:552–556.

Leach K, Conigrave AD, Sexton PM, and Christopoulos A (2015). Towards tissue-specific pharmacology: insights from the calcium-sensing receptor as a paradigm for GPCR (patho)physiological bias. *Trends Pharmacol Sci* **36**:215–225.

Leurs R, Bakker RA, Timmerman H, and de Esch IJP (2005). The histamine H3 receptor: from gene cloning to H3 receptor drugs. *Nat Rev Drug Discov* **4**:107–120.

Ligneau X, Perrin D, Landais L, Camelin JC, Calmels TPG, Berrebi-Bertrand I, Lecomte JM, Parmentier R, Anaclet C, Lin JS et al., (2007). BF2.649 [1-{3-[3-(4-Chlorophenyl)propoxy]propyl}piperidine, hydrochloride], a nonimidazole inverse agonist/antagonist at the human histamine H3 receptor: Preclinical pharmacology. *J Pharmacol Exp Ther* **320**:365–375.

Liu JJ, Horst R, Katritch V, Stevens RC, and Wüthrich K (2012). Biased signaling pathways in β2-adrenergic receptor characterized by 19F-NMR. *Science* **335**:1106–1110.

Medhurst AD, Atkins AR, Beresford IJ, Brackenborough K, Briggs MA, Calver AR, Cilia J, Cluderay JE, Crook B, Davis JB et al., (2007). GSK189254, a novel H3 receptor antagonist that binds to histamine H3 receptors in Alzheimer's disease brain and

improves cognitive performance in preclinical models. *J Pharmacol Exp Ther* **321**:1032–1045.

Morisset S, Rouleau A, Ligneau X, Gbahou F, Tardivel-Lacombe J, Stark H, Schunack W, Ganellin CR, Schwartz JC, and Arrang J-M (2000). High constitutive activity of native H3 receptors regulates histamine neurons in brain. *Nature* **408**:860–864.

Nijmeijer S, Vischer HF, Sirci F, Schultes S, Engelhardt H, de Graaf C, Rosethorne EM, Charlton SJ, and Leurs R (2013). Detailed analysis of biased histamine H4 receptor signalling by JNJ 7777120 analogues. *Br J Pharmacol* **170**:78–88.

Noetzel MJ, Gregory KJ, Vinson PN, Manka JT, Stauffer SR, Lindsley CW, Niswender CM, Xiang Z, and Conn PJ (2013). A novel metabotropic glutamate receptor 5 positive allosteric modulator acts at a unique site and confers stimulus bias to mGlu5 signaling. *Mol Pharmacol* **83**:835–847.

O'Dowd BF, Hnatowich M, Regan JW, Leader WM, Caron MG, and Lefkowitz RJ (1988). Site-directed mutagenesis of the cytoplasmic domains of the human beta 2-adrenergic receptor. Localization of regions involved in G protein-receptor coupling. *J Biol Chem* **263**:15985–15992.

Pedregosa F, Varoquaux G, Gramfort A, Michel C, Thirion B, Grisel O, Blondel M, Prettenhofer P, Weiss R, and Dubourg V et al., (2011). Scikit-learn: Machine learning in Python. *J Mach Lean Res* **12**:2825–2830.

Pillot C, Heron A, Cochois V, and Tardivel-Lacombe J (2002). A detailed mapping of the histamine H 3 receptor and its gene transcripts in rat brain. *Neuroscience* **114**(1):173–193.

Riddy DM, Valant C, Rueda P, Charman WN, Sexton PM, Summers RJ, Christopoulos A, and Langmead CJ (2015). Label-Free Kinetics: Exploiting Functional Hemi-Equilibrium to Derive Rate Constants for Muscarinic Receptor Antagonists. *Mol Pharmacol* **88**(4):779-790

Rook JM, Xiang Z, Lv X, Ghoshal A, Dickerson JW, Bridges TM, Johnson KA, Foster DJ, Gregory KJ, Vinson PN, Thompson AD, Byun N, Collier RL, Bubser M, Nedelcovych

MT, Gould RW, Stauffer SR, Daniels JS, Niswender CM, Lavreysen H, Mackie C, Conde-Ceide S, Alcazar J, Bartolomé-Nebreda JM, Macdonald GJ, Talpos JC, Steckler T, Jones CK, Lindsley CW, and Conn PJ (2015). Biased mGlu5-Positive Allosteric Modulators Provide In Vivo Efficacy without Potentiating mGlu5 Modulation of NMDAR Currents. *Neuron* **86**:1029–1040.

Sahlholm K, Nilsson J, Marcellino D, Fuxe K, and Århem P (2012). Voltage sensitivities and deactivation kinetics of histamine H_3 and H_4 receptors. *Biochim Biophys Acta* **1818**:3081–3089.

Sato M, Horinouchi T, Hutchinson DS, Evans BA, and Summers RJ (2007). Ligand-directed signaling at the beta3-adrenoceptor produced by 3-(2-Ethylphenoxy)-1-[(1,S)-1,2,3,4-tetrahydronapth-1-ylamino]-2S-2-propanol oxalate (SR59230A) relative to receptor agonists. *Mol Pharmacol* **72**:1359–1368.

Schnell D, Burleigh K, Trick J, and Seifert R (2010). No evidence for functional selectivity of proxyfan at the human histamine H3 receptor coupled to defined Gi/Go protein heterotrimers. *J Pharmacol Exp Ther* **332**:996–1005.

Schwartz J-C (2011). The histamine H3 receptor: from discovery to clinical trials with pitolisant. *Br J Pharmacol* **163**:713–721.

Shonberg J, Herenbrink CK, Lopez L, Christopoulos A, Scammells PJ, Capuano B, and Lane JR (2013). A structure-activity analysis of biased agonism at the dopamine D2 receptor. *J Med Chem* **56**:9199–9221.

Stark H, Purand K, Hüls A, Ligneau X, Garbarg M, Schwartz JC, and Schunack W (1996). [125I]iodoproxyfan and related compounds: a reversible radioligand and novel classes of antagonists with high affinity and selectivity for the histamine H3 receptor. *J Med Chem* **39**:1220–1226.

Sykes DA, Dowling MR, and Charlton SJ (2009). Exploring the mechanism of agonist efficacy: a relationship between efficacy and agonist dissociation rate at the muscarinic M3 receptor. *Mol Pharmacol* **76**:543–551.

Thompson GL, Lane JR, Coudrat T, Sexton PM, Christopoulos A, and Canals M (2015).
Biased Agonism of Endogenous Opioid Peptides at the μ-Opioid Receptor. *Mol
Pharmacol* **88**(2):335–346.

Tiligada E, Zampeli E, Sander K, and Stark H (2009). Histamine H3 and H4 receptors as
novel drug targets. *Expert Opin Investig Drugs* **18**:1519–1531.

Valant C, May LT, Aurelio L, Chuo CH, White PJ, Baltos J-A, Sexton PM, Scammells PJ,
and Christopoulos A (2014). Separation of on-target efficacy from adverse effects
through rational design of a bitopic adenosine receptor agonist. *Proc. Natl. Acad. Sci.
U.S.A.* **111**:4614–4619.

Ward RJ, Alvarez Curto E, and Milligan G (2011). Using the Flp-In™ T-Rex™ system to
regulate GPCR expression. *Methods Mol Biol* **746**:21–37.

Weichert D, Banerjee A, Hiller C, Kling RC, Hübner H, and Gmeiner P (2015). Molecular
determinants of biased agonism at the dopamine D_2 receptor. *J Med Chem* **58**:2703–
2717.

Wellendorph P, Goodman MW, Burstein ES, Nash NR, Brann MR, and Weiner DM (2002).
Molecular cloning and pharmacology of functionally distinct isoforms of the human
histamine H(3) receptor. *Neuropharmacology* **42**:929–940.

Wold S, Esbensen K, and Geladi P (1987). Principal component analysis. *Chemom Intell Lab
Syst* **2**:37–52

Footnotes

Riddy and Cook contributed equally to this manuscript

Legends for Figures

Figure 1

Structures of hH$_3$R agonists used for the study

Figure 2

Concentration response curves of the five agonists in (a) inhibition of cAMP accumulation (b) [Ca^{2+}]$_i$-mobilization, (c) pERK1/2, (d) GTPγ^{35}S binding, (e) GSK3β (f) PLA2, and (g) cell impedance assays at the hH$_3$R$_{445}$. Experiments were performed as described in the Materials and Methods section. The equations as described in the Data Analysis section were fitted to the data to estimate EC$_{50}$ and E$_{max}$ values (Supplementary Table 1) or to calculate Logτ/K_A values for the agonists (Table 1). Grouped data are shown ± SEM (n=3-7).

Figure 3

Concentration response curves of the five agonists in (a) inhibition of cAMP accumulation (b) [Ca^{2+}]$_i$-mobilization, (c) pERK1/2, (d) GTPγ^{35}S binding, (e) GSK3β (f) PLA2, and (g) cell impedance assays at the hH$_3$R$_{365}$. Experiments were performed as described in the Materials and Methods section. The equations as described in the Data Analysis section were fitted to the data to estimate EC$_{50}$ and E$_{max}$ values (Supplementary Table 2) or to calculate Logτ/K_A values for the agonists (Table 2). Grouped data are shown ± SEM (n=3-8).

Figure 4

ΔLog(τ/K_A) values for each agonist in each assay with respect to RαMH for (a) hH$_3$R$_{445}$ and (b) hH$_3$R$_{365}$ isoforms. Data represent the mean ± SEM (n=3-8). For hH$_3$R$_{445,}$ two-way ANOVA of ΔLog(τ/K_A) values revealed a significant effect of both agonist (P = 0.004) and assay (P = 0.002), but no interaction (P = 0.22). For hH$_3$R$_{365}$ there was a highly significant effect of agonists (P < 0.0001) and assay (P < 0.0001) and a very significant interaction

34

between the two variables ($P = 0.0008$). For Tukey's planned comparisons testing: * $P <$ 0.05, ** $P < 0.01$, *** $P < 0.001$ between agonists for the same assay; ^ $P < 0.05$, ^^ $P <$ 0.01, ^^^ $P < 0.001$ between assays for the same agonist.

Figure 5

Webs of bias of agonist-stimulated responses of a range of histamine agonists for (a) hH_3R_{445} and (b) hH_3R_{365} isoforms normalised to the values obtained for the reference agonist RαMH (axes represent $\Delta Log(\tau/K_A)$). Webs of bias of agonist-stimulated responses values at (c) hH_3R_{445} and (d) hH_3R_{365} isoforms normalised to the values obtained for the reference pathway, cAMP (axes represent $\Delta\Delta Log(\tau/K_A)$). Values used to plot these webs are shown in Tables 1 & 2 in parentheses.

Figure 6

Comparison of $Log(\tau/K_A)$ values for each agonist in each assay between the different isoforms. Values > 0 denote bias towards hH_3R_{445}, whilst values < 0 denote bias towards hH_3R_{365}. Grouped data are shown $\pm$ SEM (n=3-8). Statistical significance was deemed by one sample t-test (* $P < 0.05$, ** $P < 0.01$ compared to zero i.e. no isoform bias).

Figure 7

Principal component analysis (PCA) of the calculated $\Delta\Delta Log(\tau/K_A)$ bias factors for (a) hH_3R_{445} and (b) hH_3R_{365} receptor isoforms in response to a range of agonists across the different functional assays, with data being normalised to the values obtained for RαMH and to cAMP as the reference pathway.

Molecular Pharmacology Fast Forward. Published on November 18, 2016 as DOI: 10.1124/mol.116.106153
This article has not been copyedited and formatted. The final version may differ from this version.

MOL #106153

Tables

Table 1. Logτ/K_A, ΔLogτ/K_A (normalized to RαMH), and ΔΔLogτ/K_A (normalized to cAMP), values for the hH$_3$R$_{445}$ isoform as determined from the different signaling assays. Data are expressed as mean ± SEM from a single fit to grouped data of the indicated number (N=) of individual experiments, and *n* is the transducer slope determined from shared analysis. Values in parentheses were used to plot the webs of bias presented in Figure 5.

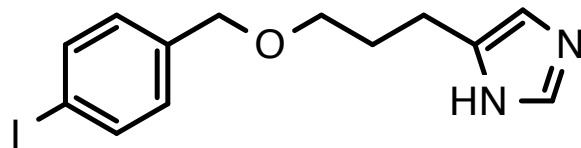|	Analysis	N=	*n*	RαMH	Imetit	NαMH	Proxyfan	Iodoproxyfan
cAMP	Logτ/K$_A$	3-7	0.85 ± 0.18	11.62 ± 0.36	10.98 ± 0.32	12.04 ± 0.28	10.07 ± 0.28	10.98 ± 0.47
	ΔLogτ/K$_A$ vs RαMH			0.00 ± 0.46	-0.64 ± 0.45	0.42 ± 0.43	-1.55 ± 0.43	-0.64 ± 0.57
	ΔΔLogτ/K$_A$ vs cAMP			0.00 ± 0.65 (1.0)	0.00 ± 0.64 (1.0)	0.00 ± 0.61 (1.0)	0.00 ± 0.60 (1.0)	0.00 ± 0.80 (1.0)
[Ca^{2+}]$_i$-mobilization	Logτ/K$_A$	4-5	0.79 ± 0.17	9.32 ± 0.17	9.61 ± 0.24	9.54 ± 0.23	8.31 ± 0.21	9.27 ± 0.39
	ΔLogτ/K$_A$ vs RαMH			0.00 ± 0.25	0.29 ± 0.29	0.22 ± 0.29	-1.01 ± 0.27	-0.04 ± 0.43
	ΔΔLogτ/K$_A$ vs cAMP			0.00 ± 0.52 (1.0)	0.93 ± 0.54 (8.5)	-0.20 ± 0.52 (0.6)	0.54 ± 0.51 (3.5)	0.60 ± 0.71 (4.0)
pERK1/2	Logτ/K$_A$	3-4	1.10 ± 0.11	10.73 ± 0.16	11.14 ± 0.04	10.63 ± 0.07	10.01 ± 0.10	10.69 ± 0.07
	ΔLogτ/K$_A$ vs RαMH			0.00 ± 0.22	0.41 ± 0.16	-0.10 ± 0.17	-0.72 ± 0.18	0.04 ± 0.17
	ΔΔLogτ/K$_A$ vs cAMP			0.00 ± 0.51 (1.0)	1.05 ± 0.48 (11.1)	-0.52 ± 0.46 (0.3)	0.82 ± 0.46 (6.7)	0.60 ± 0.59 (4.0)
GTPγ^{35}S binding	Logτ/K$_A$	3	0.82 ± 0.08	10.65 ± 0.03	10.58 ± 0.04	10.06 ± 0.08	9.44 ± 0.21	10.85 ± 0.07
	ΔLogτ/K$_A$ vs RαMH			0.00 ± 0.04	-0.07 ± 0.05	-0.59 ± 0.09	-1.21 ± 0.21	0.21 ± 0.07
	ΔΔLogτ/K$_A$ vs cAMP			0.00 ± 0.46 (1.0)	0.57 ± 0.46 (3.7)	-1.01 ± 0.44 (0.1)	0.34 ± 0.48 (2.2)	0.85 ± 0.57 (7.0)
pGSK3β	Logτ/K$_A$	3	0.87 ± 0.26	10.30 ± 0.18	11.21 ± 0.08	10.67 ± 0.41	11.16 ± 0.72	11.17 ± 0.65
	ΔLogτ/K$_A$ vs RαMH			0.00 ± 0.25	0.92 ± 0.19	0.37 ± 0.45	0.86 ± 0.74	0.87 ± 0.67
	ΔΔLogτ/K$_A$ vs cAMP			0.00 ± 0.52 (1.0)	1.56 ± 0.49 (36.0)	-0.05 ± 0.62 (0.9)	2.41 ± 0.85 (258.8)	1.52 ± 0.88 (32.7)
[^{3}H]-arachidonic acid	Logτ/K$_A$	3-4	0.60 ± 0.45	10.87 ± 0.51	ND	ND	10.05 ± 0.37	ND
	ΔLogτ/K$_A$ vs RαMH			0.00 ± 0.72			-0.82 ± 0.63	
	ΔΔLogτ/K$_A$ vs cAMP			0.00 ± 0.85 (1.0)			0.73 ± 0.76 (5.3)	
Label-free	Logτ/K$_A$	3-5	0.77 ± 0.15	8.31 ± 0.37	8.21 ± 0.22	8.51 ± 0.07	8.21 ± 0.39	9.84 ± 0.52
	ΔLogτ/K$_A$ vs RαMH			0.00 ± 0.52	-0.10 ± 0.43	0.20 ± 0.37	-0.10 ± 0.54	1.53 ± 0.64
	ΔΔLogτ/K$_A$ vs cAMP			0.00 ± 0.69 (1.0)	0.54 ± 0.62 (3.5)	-0.22 ± 0.57 (0.6)	1.45 ± 0.68 (28.1)	2.17 ± 0.85 (147.9)

ND = not determined

36

Downloaded from molpharm.aspetjournals.org at ASPET Journals on May 11, 2021

Table 2. Logτ/K_A, ΔLogτ/K_A (normalized to RαMH), and ΔΔLogτ/K_A (normalized to cAMP), values for the hH$_3$R$_{365}$ isoform as determined from the different signaling assays. Data are corrected for differences in receptor expression as determined by saturation isotherms of [^{3}H]-N-α-methyl-histamine and are expressed as mean ± SEM from a single fit to grouped data of the indicated number (N=) of individual experiments. *n* is the transducer slope determined from shared analysis. Values in parentheses were used to plot the webs of bias presented in Figure 5.

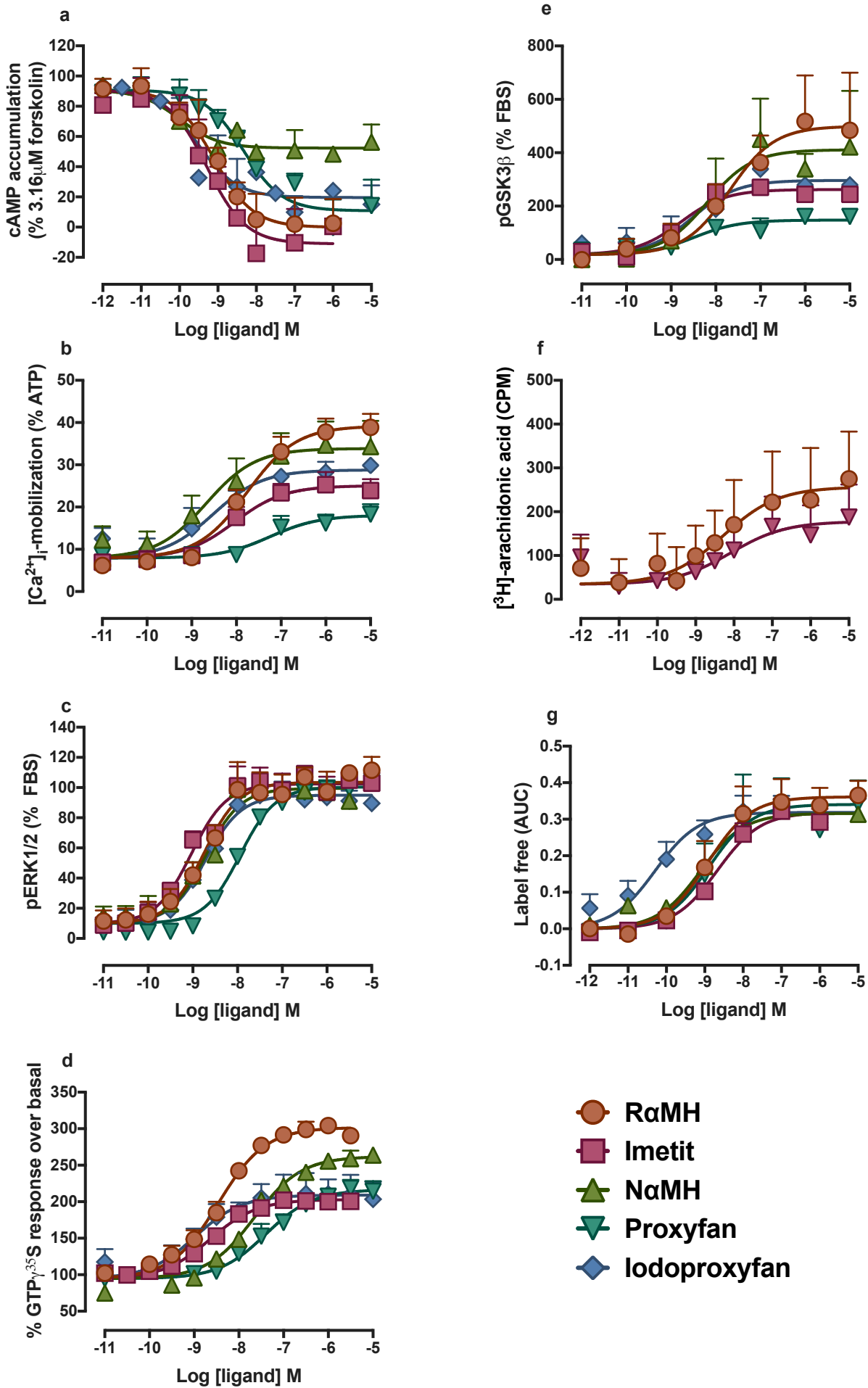|	Analysis	N=	*n*	RαMH	Imetit	NαMH	Proxyfan	Iodoproxyfan
cAMP	Logτ/K_A	5-8	0.73 ± 0.11	10.52 ± 0.19	12.39 ± 0.40	11.33 ± 0.35	9.80 ± 0.19	11.33 ± 0.14
	ΔLogτ/K_A vs RαMH			0.00 ± 0.27	1.87 ± 0.44	0.81 ± 0.40	-0.72 ± 0.27	0.81 ± 0.24
	ΔΔLogτ/K_A vs cAMP			0.00 ± 0.53 (1.0)	0.00 ± 0.63 (1.0)	0.00 ± 0.58 (1.0)	0.00 ± 0.51 (1.0)	0.00 ± 0.62 (1.0)
[Ca^{2+}]$_i$-mobilization	Logτ/K_A	3-4	1.00 ± 0.43	9.23 ± 0.50	8.92 ± 0.20	9.95 ± 0.31	NE	NE
	ΔLogτ/K_A vs RαMH			0.00 ± 0.71	-0.31 ± 0.54	0.72 ± 0.59	-3.0	-3.0
	ΔΔLogτ/K_A vs cAMP			0.00 ± 0.84 (1.0)	-2.18 ± 0.70 (0.01)	-0.09 ± 0.73 (0.8)	n/a	n/a
pERK1/2	Logτ/K_A	3-5	0.93 ± 0.12	10.29 ± 0.29	11.22 ± 0.19	10.26 ± 0.13	9.16 ± 0.41	9.75 ± 0.10
	ΔLogτ/K_A vs RαMH			0.00 ± 0.41	0.93 ± 0.35	-0.03 ± 0.32	-1.14 ± 0.50	-0.55 ± 0.31
	ΔΔLogτ/K_A vs cAMP			0.00 ± 0.61 (1.0)	-0.94 ± 0.57 (0.1)	-0.84 ± 0.53 (0.1)	-0.42 ± 0.66 (0.4)	-1.36 ± 0.65 (0.04)
GTPγ^{35}S binding	Logτ/K_A	3	0.68 ± 0.13	10.74 ± 0.33	11.45 ± 0.03	10.10 ± 0.24	9.77 ± 0.06	11.16 ± 0.04
	ΔLogτ/K_A vs RαMH			0.00 ± 0.47	0.71 ± 0.34	-0.65 ± 0.41	-0.97 ± 0.34	0.36 ± 0.34
	ΔΔLogτ/K_A vs cAMP			0.00 ± 0.66 (1.0)	-1.16 ± 0.56 (0.1)	-1.45 ± 0.59 (0.04)	-0.25 ± 0.55 (0.6)	-0.45 ± 0.66 (0.4)
pGSK3β	Logτ/K_A	3	NE	NE	NE	NE	NE	NE
	ΔLogτ/K_A vs RαMH							
	ΔΔLogτ/K_A vs cAMP							
[^{3}H]-arachidonic acid	Logτ/K_A	4	0.43 ± 0.20	10.73 ± 0.17	ND	ND	9.65 ± 0.40	ND
	ΔLogτ/K_A vs RαMH			0.00 ± 0.25			-1.08 ± 0.43	
	ΔΔLogτ/K_A vs cAMP			0.00 ± 0.52 (1.0)			0.03 ± 0.61 (1.1)	
Label-free	Logτ/K_A	3-4	0.78 ± 0.20	8.21 ± 0.24	8.07 ± 0.53	8.61 ± 0.46	7.74 ± 0.14	8.41 ± 0.62
	ΔLogτ/K_A vs RαMH			0.00 ± 0.33	-0.14 ± 0.58	0.40 ± 0.52	-0.47 ± 0.27	0.21 ± 0.66
	ΔΔLogτ/K_A vs cAMP			0.00 ± 0.57 (1.0)	-2.01 ± 0.74 (0.01)	-0.41 ± 0.67 (0.4)	0.25 ± 0.51 (1.8)	-0.60 ± 0.87 (0.2)

ND = not determined, NE = no effect

37

Figure 1

(R)-α-methyl histamine (RαMH)

Imetit

(N)-α-methyl histamine (NαMH)
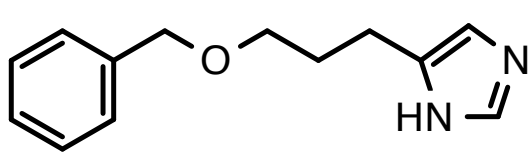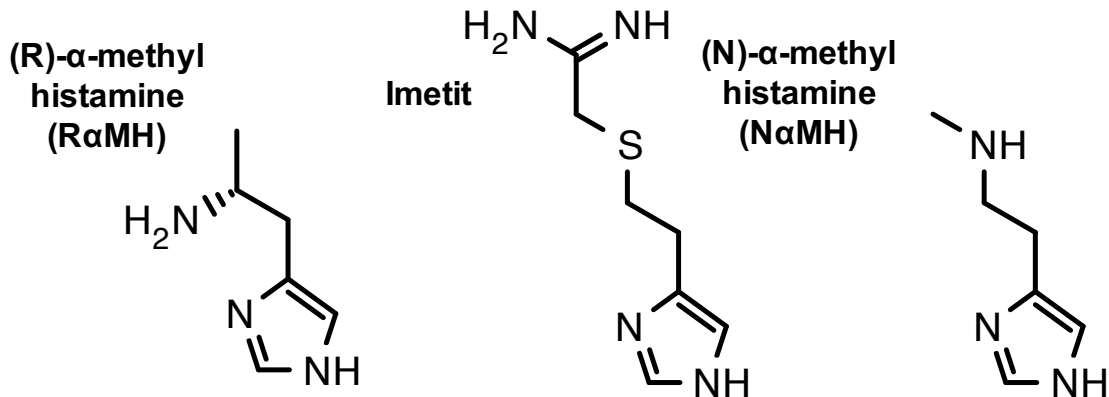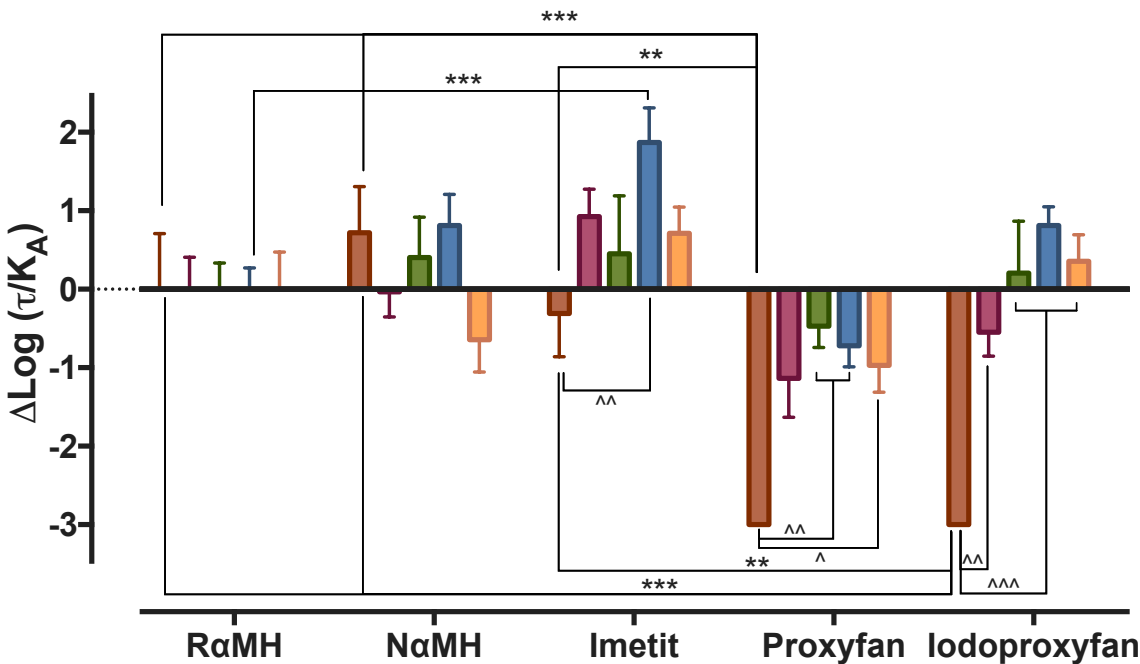
Proxyfan

Iodoproxyfan

Figure 2

hH_3R_{445}

Figure 3

hH₃R₃₆₅
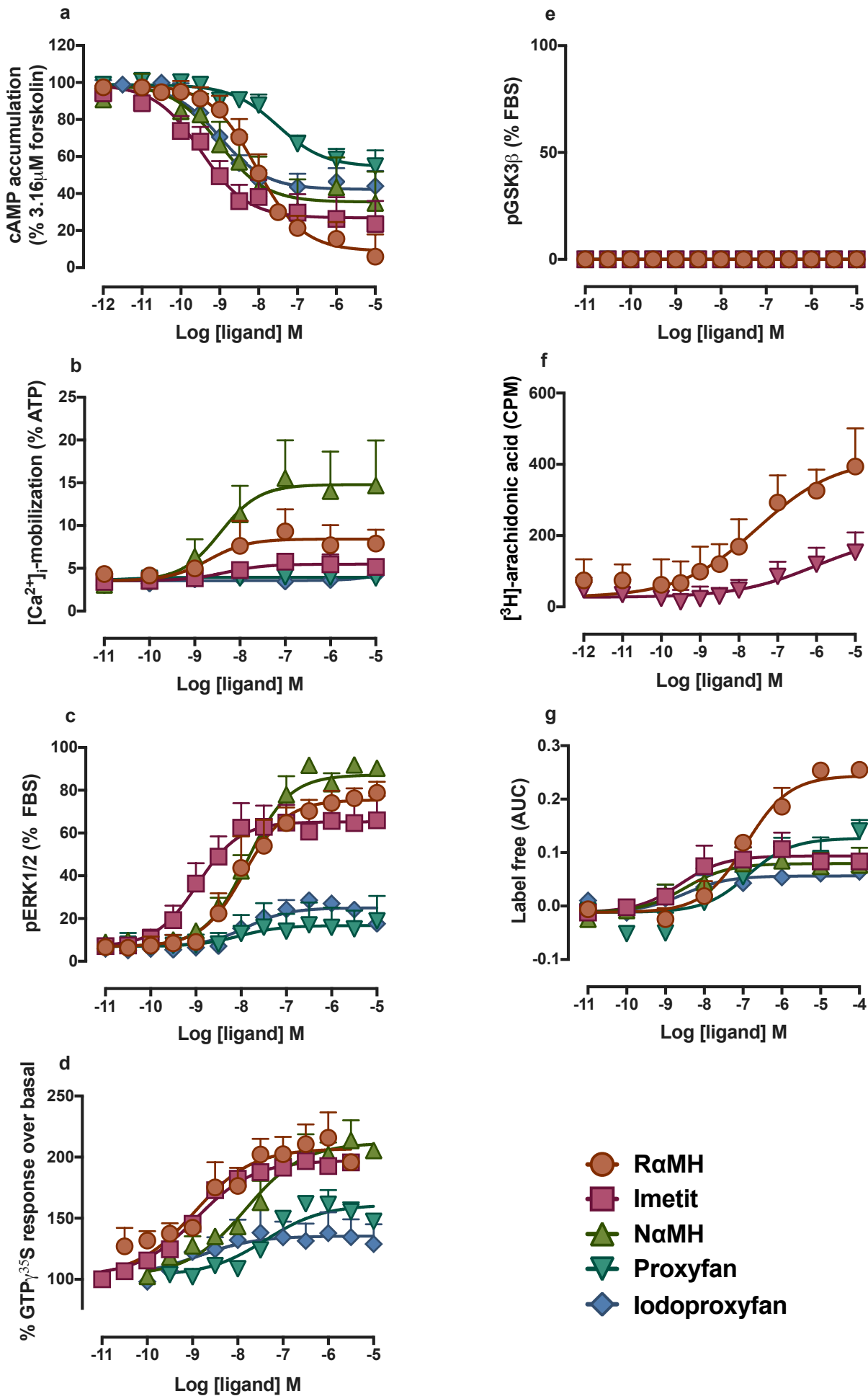
Figure 4
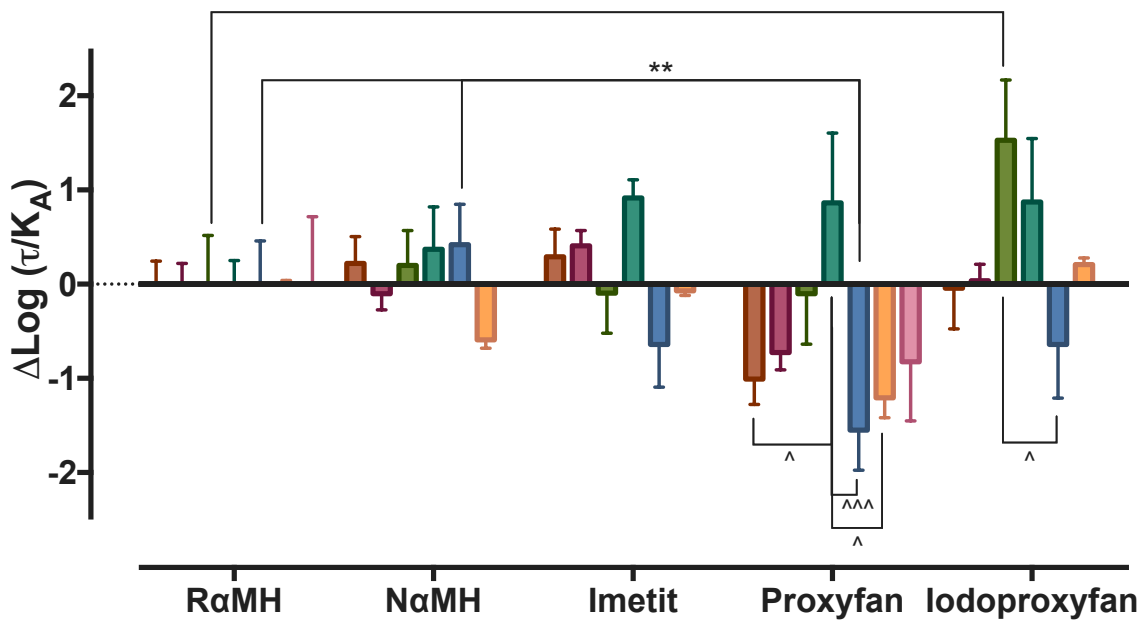
Figure 5

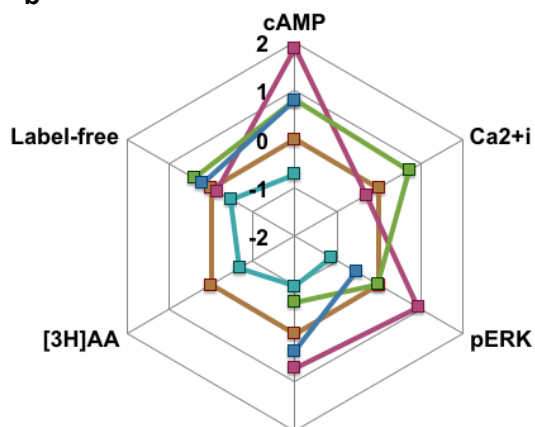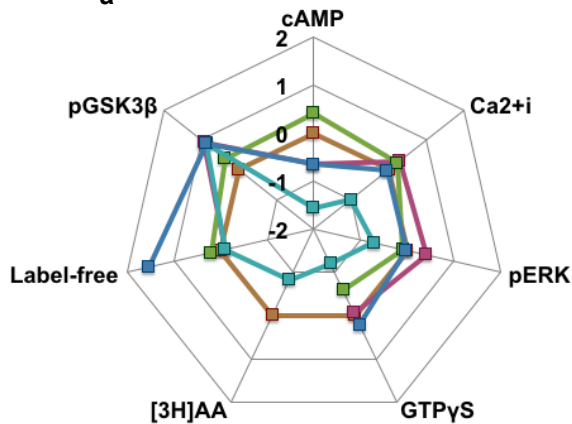hH_3R_{445}

hH_3R_{365}
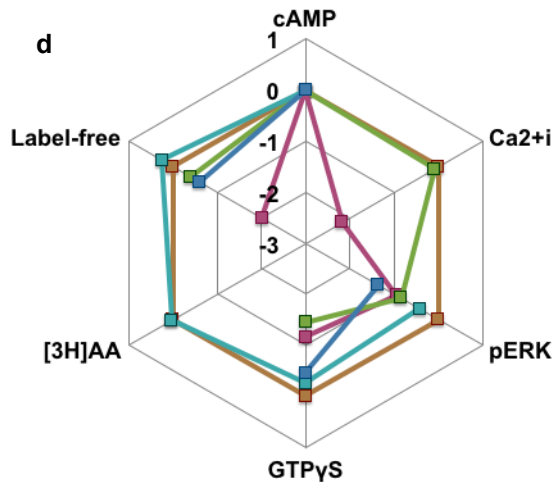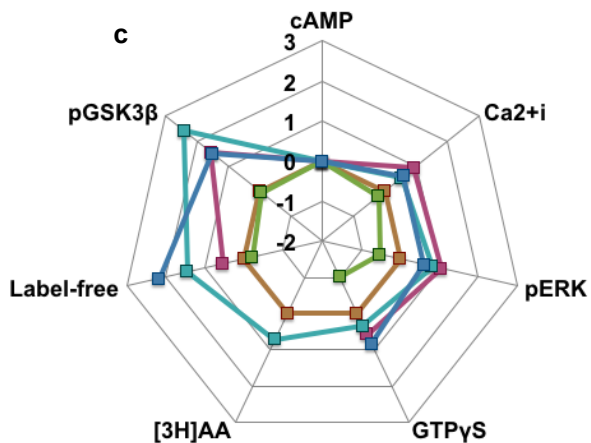
$\Delta\text{Log}(\tau/K_A)$

$\Delta\Delta\text{Log}(\tau/K_A)$
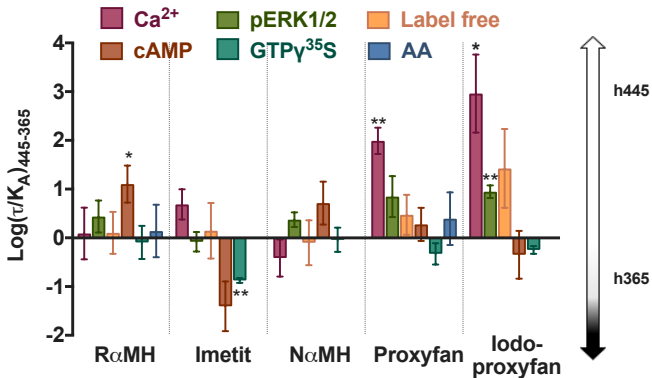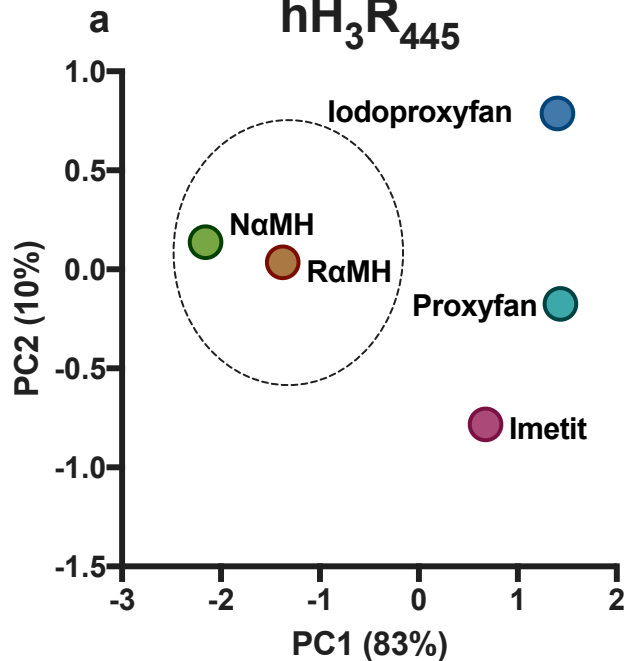
RαMH — Imetit — NαMH — Proxyfan — Iodoproxyfan

Figure 6

Figure 7